Interaction-induced directional transport on periodically driven chains

Helena Drüeke [*] and Dieter Bauer [†]
Institute of Physics, University of Rostock, 18051 Rostock, Germany

(Received 16 October 2023; revised 16 January 2024; accepted 21 February 2024; published 8 April 2024)

We study a driven system in which interaction between particles causes their directional, coupled movement. In that model system, two particles move alternatingly in time on two coupled chains. Without interaction, both particles diffuse along their respective chains, independent from one another. Interaction between them, whether attractive or repellent, leads to an energetic separation of configurations where the particles are close to each other and those where they are farther separated. The energy difference causes close-by particles to remain bound together, forming a doublon. Their relative position in the starting configuration determines whether the doublon moves to the left or right or remains stationary due to the periodic driving.

DOI: 10.1103/PhysRevResearch.6.023032

I. INTRODUCTION

Directional transport in physical systems can be realized in various ways. The most obvious one is applying an external field, e.g., an electric field that accelerates a charged particle in a particular direction or an inhomogeneous magnetic field that deflects atoms in different directions according to their spin. An alternating electric field can also lead to directional transport. A simple example is an electron emitted at, say, $t = 0$ into a linearly polarized laser field, e.g., by ionization. Depending on the emission time, the electron may drift in opposite directions, parallel to the polarization of the incident laser field. Other ways to achieve directional transport are by topologically protected edge currents through the breaking of time-reversal symmetry, e.g., by a magnetic field or spin-orbit coupling [Hall effect(s) [1–4]], or by periodic driving and asymmetric potentials [(semi)classical [5,6] and quantum ratchets [7–9], and Thouless pumping [10,11]]. All these systems prescribe the direction of movement of particles within them. Interactions between the particles will affect the particle dynamics, but as long as the particle interaction is symmetric under particle exchange, one would not expect directional transport to arise. In fact, one might expect that interaction, in general, would broaden momentum distributions, including peaks in such distributions that correspond to directional motion without interaction. The directional motion would then gradually disappear with increasing interaction strength. However, it has been shown recently that topologically protected motion survives to a certain extent in a Hubbard-Thouless pump [12]. Interaction might even be required to achieve directional transport in a topological many-body system [13].

In this work, we present a minimal model of a driven two-particle system that shows directional transport due to interaction, even though this interaction is symmetric under particle exchange. Moreover, the drive is spatially symmetric (unlike the laser example above) and no asymmetric potentials are involved (in contrast to the ratchet systems). Therefore, the direction of movement is not predetermined by the system parameters and depends on the initial condition.

The key to directional transport in our system is the alternating driving of the two particles. While the interaction in our model system is always active, the hopping of each particle is only allowed for half of the driving period. In this case, the initial configuration determines the direction in which the bound pair of particles (i.e., doublon) moves. Without interaction, the doublon does not exist and the two particles simply diffuse independently without preferred directionality. The alternating drive where only one of the two particles is allowed to move per half period implies that the two particles are distinguishable and should be independently addressable by external fields. Lin, Ke, and Lee [14] investigated a system similar to the one described in this work, as well as its implementation in ultracold atoms in optical lattices (see Sec. IV). Their two spin-1/2 particles experience different one-dimensional trapping lattices because one is spin-up and the other spin-down. In contrast to our work presented in this publication, the interaction between neighboring particles is not isotropic. By tuning hopping and interaction strengths, the two particles form topological bound states. Periodic modulation of these two parameters leads to topological Thouless pumping of the bound states. Without interaction, however, the system in [14] is topologically trivial and no transport occurs.

A related phenomenon is Coulomb drag [15], where a current in one conductor induces a current in a second, adjacent, but electrically isolated conductor. In our system, the two particles behave similarly but drag each other reciprocally without an external bias (voltage) on either conductor.

This publication consists of the following parts. We introduce the model in Sec. II and explore the behavior of one particle during half its driving period in Sec. III. The doublon dynamics can be conveniently analyzed by mapping

[*] helena.drueeke@uni-rostock.de
[†] dieter.bauer@uni-rostock.de

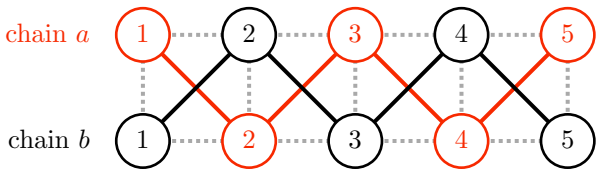

FIG. 1. Chains a and b of identical length $N = 5$ (we chose this small N for illustration purposes but performed all calculations with much longer chains). The red and black lines indicate the hopping J of particles a and b on their respective chains. Dashed gray lines indicate the interaction V between nearest-neighbor sites on different chains.

onto a 2D system, as discussed in Sec. IV. Section V describes possible experimental implementations. Finally, we conclude and discuss the significance of our work in Sec. VI.

We use units in which $\hbar = 1$.

II. SYSTEM

We consider the lattice shown in Fig. 1, consisting of two chains a and b of length N with one particle on each chain (also labeled a and b). Each particle may hop along its respective chain; hoppings to the other chain are prohibited. The particles move alternatingly, starting with particle a. The interaction between particles is between nearest neighbors, i.e., across the chains.

The Hamiltonian reads

$$\hat{H}(t) = \sum_{\langle i,j\rangle} (J_a(t)\hat{a}_i^\dagger \hat{a}_j + J_b(t)\hat{b}_i^\dagger \hat{b}_j) + V \sum_{\langle\langle i,j\rangle\rangle} \hat{n}_i^{(a)}\hat{n}_j^{(b)}, \quad (1)$$

where $\hat{a}_i$ and $\hat{b}_i$ are annihilation operators on site i of chains a and b, respectively, $\hat{a}_i^\dagger$ and $\hat{b}_i^\dagger$ are the corresponding creation operators, and $\hat{n}_i^{(a)} = \hat{a}_i^\dagger \hat{a}_i$ and $\hat{n}_j^{(b)} = \hat{b}_j^\dagger \hat{b}_j$ are the occupation number operators. $\langle i, j\rangle$ indicates nearest neighbors within a chain and $\langle\langle i, j\rangle\rangle$ nearest neighbors across the chains.

The hoppings $J_{a,b}(t)$ are assumed to be periodic with a period T and piecewise constant,

$$J_a(t) = \begin{cases} J, & 0 \leqslant t < T/2, \\ 0, & T/2 \leqslant t < T, \end{cases} \quad (2a)$$

$$J_b(t) = \begin{cases} 0, & 0 \leqslant t < T/2, \\ J, & T/2 \leqslant t < T. \end{cases} \quad (2b)$$

We choose $J = 1$ in all numerical calculations throughout this publication. With the labeling in Fig. 1, we can write

$$\hat{H}(t) = \sum_{i=1}^{N-1} \left((J_a(t)\hat{a}_i^\dagger \hat{a}_{i+1} + J_b(t)\hat{b}_i^\dagger \hat{b}_{i+1}) + \text{H.c.} \right.$$
$$\left. + V\left(\hat{n}_i^{(a)}\hat{n}_{i+1}^{(b)} + \hat{n}_{i+1}^{(a)}\hat{n}_i^{(b)}\right)\right) + V \sum_{i=1}^{N} \hat{n}_i^{(a)}\hat{n}_i^{(b)}. \quad (3)$$

III. MOVEMENT OF ONE PARTICLE DURING A HALF PERIOD

We investigate particle a's movement on its chain a during the first half period ($0 \leqslant t < T/2$). Particle a starts in site i and propagates. Particle b is located in site j and remains stationary during this time.

The Hamiltonian during this phase can be written as an $N \times N$ matrix

$$H = H_J + H_V. \quad (4)$$

It consists of two parts, one describing the hopping

$$H_J = \text{tridiag}(J, 0, J) = \begin{pmatrix} 0 & J & & 0 \\ J & 0 & \ddots & \\ & \ddots & \ddots & J \\ 0 & & J & 0 \end{pmatrix} \quad (5)$$

and one describing the interaction

$$H_V = (v_{k,l}), \quad (6)$$

with

$$v_{k,l} = \begin{cases} V, & k = l = j-1, j, j+1, \\ 0, & \text{else} \end{cases} \quad (7)$$

on sites neighboring the position j of particle b.

A. $|V| \gg J$

The interaction between particles is between neighboring sites, i.e., for states with $|i - j| \leqslant 1$. Therefore, a strong potential $|V| \gg J$ leads to a large energetic separation of the states $i = j - 1, j, j + 1$ from the others. If particle a starts its movement in a site i with $i < j - 1$ ($i > j + 1$), it cannot bridge this energy gap and will remain on the left side of particle b, $i < j - 1$ (right side, $i > j + 1$). Interestingly, it does not matter if the potential is repulsive ($V > 0$) or attractive ($V < 0$).

Assuming $|i - j| \leqslant 1$ with a strong potential $|V| \gg J$ confines particle a to the three sites $j - 1$, j, and $j+1$. The $N\times N$ Hamiltonian (4) becomes limited to these three states (3×3),

$$H = \begin{pmatrix} V & J & 0 \\ J & V & J \\ 0 & J & V \end{pmatrix}, \quad (8)$$

with eigenenergies

$$E_0 = V, \quad E_{1,2} = V \pm \sqrt{2}J \quad (9)$$

and eigenstates

$$\varphi_0 = \begin{pmatrix} 1 \\ 0 \\ -1 \end{pmatrix}, \quad \varphi_{1,2} = \begin{pmatrix} 1 \\ \pm\sqrt{2} \\ 1 \end{pmatrix}. \quad (10)$$

We can now write any time-dependent state as

$$\psi(t) = \sum_{h=0}^{2} c_h \exp(-\mathrm{i}E_h t)\varphi_h. \quad (11)$$

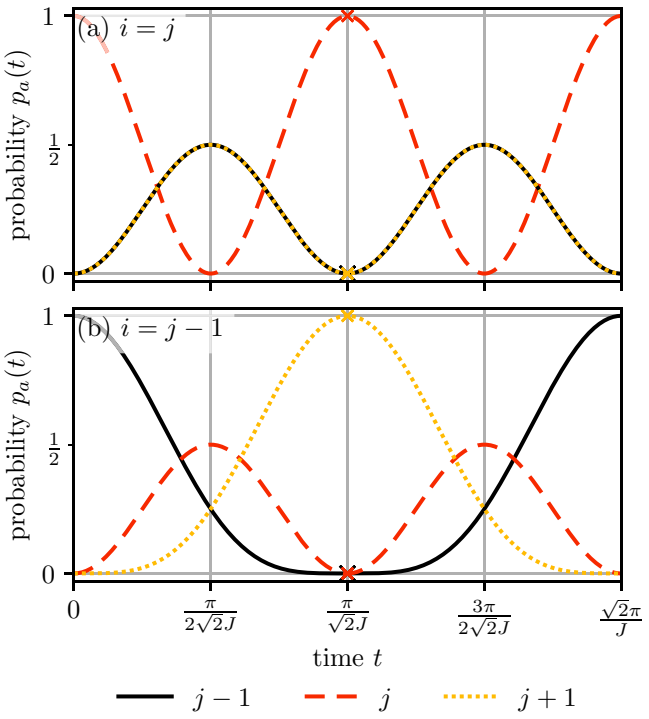

FIG. 2. Probabilities of particle a on different sites as a function of time with $|V| \gg J$ (a) for starting position $i = j$ and (b) for starting position $i = j - 1$. The crosses mark the probabilities at the end of the driving phase $t_a = \frac{\pi}{\sqrt{2}J}$.

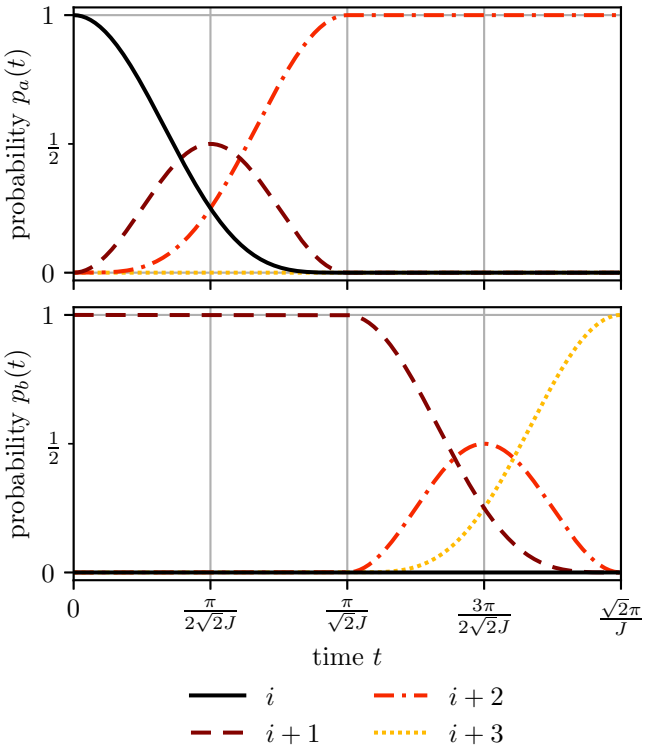

FIG. 3. Probabilities of particles a and b on different sites as a function of time. Particle a moves from site i via site $i+1$ to site $i+2$ during the first phase; then particle b moves from site $i+1$ via site $i+2$ to site $i+3$ during the second phase.

1. $i = j$

If particle a starts at $i = j$, $\psi_a(0) = (0, 1, 0)^\mathsf{T}$, the coefficients are $c_0 = 0$ and $c_{1,2} = \pm\frac{1}{2\sqrt{2}}$, resulting in

$$\psi_a(t) = \frac{\exp(-\mathrm{i}Vt)}{\sqrt{2}\mathrm{i}} \begin{pmatrix} \sin(\sqrt{2}Jt) \\ \sqrt{2}\mathrm{i}\,\cos(\sqrt{2}Jt) \\ \sin(\sqrt{2}Jt) \end{pmatrix}. \tag{12}$$

The probability at the three sites $i = j-1, j, j+1$ is

$$p_a(t) = |\psi_a(t)|^2 = \frac{1}{2} \begin{pmatrix} \sin^2(\sqrt{2}Jt) \\ 2\,\cos^2(\sqrt{2}Jt) \\ \sin^2(\sqrt{2}Jt) \end{pmatrix}, \tag{13}$$

shown in Fig. 2(a). The particle moves symmetrically from the starting site j to the left and right neighbors $j \pm 1$, where it reaches a maximum probability of 0.5 at time $t = \frac{\pi}{2\sqrt{2}J}$ before completely returning to site j at $t = \frac{\pi}{\sqrt{2}J}$.

2. $i = j - 1$

If particle a starts at $i = j - 1$, $\psi_a(0) = (1, 0, 0)^\mathsf{T}$, the coefficients are $c_0 = \frac{1}{2}$ and $c_{1,2} = \frac{1}{4}$, resulting in

$$\psi_a(t) = \frac{\exp(-\mathrm{i}Vt)}{2} \begin{pmatrix} 1 + \cos(\sqrt{2}Jt) \\ -\sqrt{2}\mathrm{i}\,\sin(\sqrt{2}Jt) \\ -1 + \cos(\sqrt{2}Jt) \end{pmatrix}. \tag{14}$$

The probability is

$$p_a(t) = \begin{pmatrix} \cos^4(Jt/\sqrt{2}) \\ \sin^2(\sqrt{2}Jt)/2 \\ \sin^4(Jt/\sqrt{2}) \end{pmatrix}, \tag{15}$$

shown in Fig. 2(b).

We choose $t_a = \frac{\pi}{\sqrt{2}J}$ to achieve a complete transfer of particle a from site $j-1$ to site $j+1$. Particle a leapfrogs over particle b from its left to right neighbor. If we choose the timing of the second phase of the driving cycle as $t_b = \frac{\pi}{\sqrt{2}J}$, particle b will leapfrog over particle a, leading to directional transport. Effectively, both particles move two sites to the right without spreading. Figure 3 shows the probabilities $p_a(t)$ and $p_b(t)$ for the complete cycle. Figure 4 shows a sketch of the particles' movement.

3. $i = j + 1$

If particle a starts at $i = j + 1$, $\psi_{i=j+1}(0) = (0, 0, 1)^\mathsf{T}$, it will analogously leapfrog over particle b to site $j - 1$, resulting in directional transport to the left.

B. $V = 0$

For potential $V = 0$, the position j of particle b does not influence particle a's movement. The Hamiltonian (4) simplifies

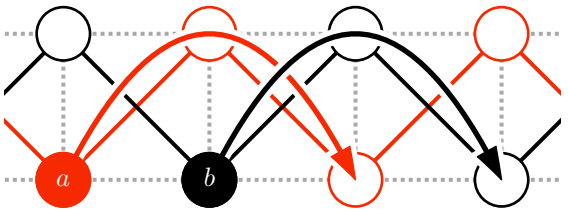

FIG. 4. Sketch of the leapfrogging movement of particles a and b during a complete driving cycle. During the first phase ($0 \leqslant t < T/2$), particle a jumps over particle b and two sites to the right. Then, during the second phase ($T/2 \leqslant t < T$), particle b jumps over particle a and two sites to the right.

to

$$H = H_J = \text{tridiag}(J, 0, J) = \begin{pmatrix} 0 & J & & 0 \\ J & 0 & \ddots & \\ & \ddots & \ddots & J \\ 0 & & J & 0 \end{pmatrix}. \quad (16)$$

The time-dependent Schrödinger equation

$$\mathrm{i}\partial_t \psi_a(t) = \hat{H}\psi_a(t) \quad (17)$$

leads to a diffusion-type equation for the time-dependent wave function $\psi(n,t)$ in site n,

$$\partial_t \psi_a(n,t) = -\mathrm{i}J(\psi_a(n-1,t) + \psi_a(n+1,t)). \quad (18)$$

For a particle starting in site i on an infinitely long chain, it follows [16] that

$$\psi_a(i+l,t) = \mathrm{i}^{-l}\mathcal{J}_l(2Jt) \quad (19)$$

and

$$p_a(i+l,t) = |\psi_a(i+l,t)|^2 = \mathcal{J}_l^2(2Jt), \quad (20)$$

where $\mathcal{J}_l$ is the Bessel function of the first kind.

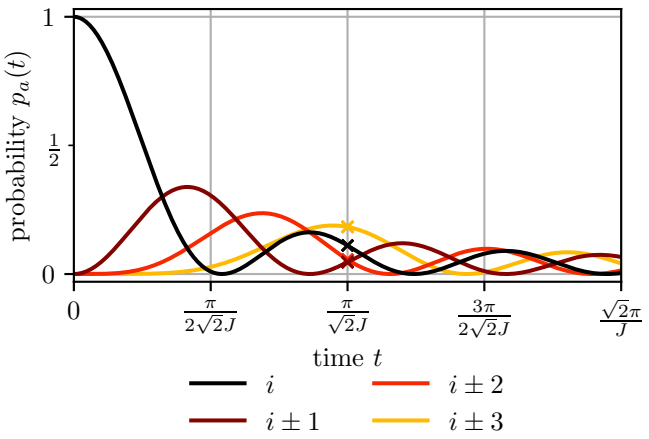

FIG. 5. Probabilities of particle a on different sites as a function of time with $V = 0$. The crosses mark the probabilities at the end of the driving phase $t_a = \frac{\pi}{\sqrt{2}J}$.

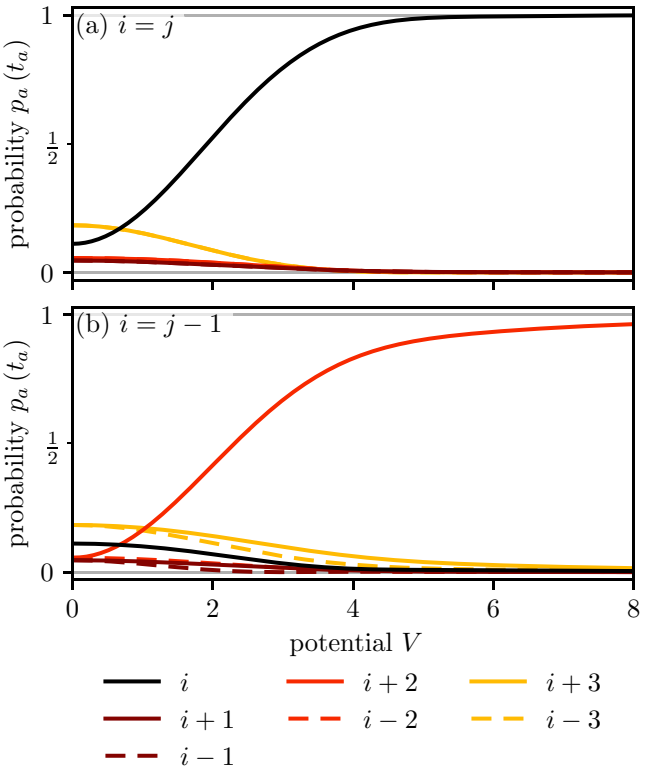

FIG. 6. Probabilities of particle a on different sites at time $t_a = \frac{\pi}{\sqrt{2}J}$ as a function of interaction V (a) for starting position $i = j$ and (b) for starting position $i = j - 1$.

The probabilities $p_a(t)$ are shown in Fig. 5. Particle a spreads symmetrically to the left and the right. This proves that, without interaction between the particles ($V = 0$), no doublons can exist and neither the stationary nor leapfrogging state occurs.

C. $V \neq 0$

For potential $V \neq 0$ but not $V \gg J$, we have to use the whole Hamiltonian (4) to describe the system.

A video in the Supplemental Material [17] shows the evolution of the probabilities for increasing interaction V going from the spreading at $V = 0$ shown in Fig. 5 to the periodic returns at $V \gg J$ shown in Fig. 2. We are mainly interested in the probabilities at the end of phase a, $t_a = \frac{\pi}{\sqrt{2}J}$. These are marked by crosses in Figs. 2 and 5. Figure 6 shows the probabilities $p(t_a)$ as a function of the interaction V. Even at relatively small interactions $V \gtrapprox 6$, the initial configuration $i = j$ remains stationary, $p_{i=j}(t_a) \approx 1$. The leapfrogging state (starting at $i = j \pm 1$) needs higher interaction strengths $V \gtrapprox 20$ to remain localized [$p_{j\mp1}(t_a) \approx 1$] while jumping from site $j \pm 1$ to site $j \mp 1$.

IV. MAPPING TO 2D

We map the two chains to a square grid, as shown in Fig. 7. The positions i and j of particles a and b are plotted along the horizontal and vertical directions, respectively.

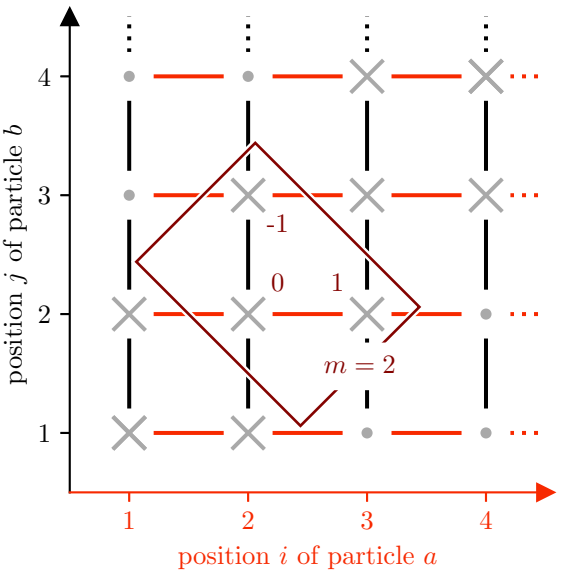

FIG. 7. Mapping of the Hamiltonian to a 2D lattice with the two particles' indices along the two axes (a-chain index s at the x axis; b-chain index t at the y axis). Red and black lines connecting sites indicate the time-dependent hoppings $J_a(t)$ and $J_b(t)$. Gray crosses indicate the combinations of lattice sites for which the interaction potential is nonvanishing. These form the reduced lattice on which the doublon dynamics take place if $V \gg J_{a,b}$. The unit cell of this three-site-wide ribbon and the new labeling $i - j = 1, 0, -1$ are indicated in brown.

A. Interacting subsystem for $V \gg J$

For strong interactions $V \gg J$, interacting states (located on sites marked by crosses in Fig. 7) are energetically separated from noninteracting states (located on sites marked by dots). If the initial state is interacting, it will remain an interacting state. Hence, for $V \gg J$, we only need to consider a subset of the 2D system, as indicated by the brown unit cell. This reduced system is quasi-1D, effectively a three-site wide ribbon. The unit cell m contains three sites, labeled by the difference of positions a and b, $i - j = 1, 0$, and -1.

1. Stationary states

A state initially located at site $(m, 0)$ will split towards sites $(m-1, -1)$ and $(m, 1)$ during the first phase, returning to $(m, 0)$ at the end of the phase, $t_a = \frac{\pi}{\sqrt{2}J}$. During the second phase, it will equivalently split towards sites $(m, -1)$ and $(m-1, 1)$ before returning to $(m, 0)$ at the end of the driving cycle $T = t_a + t_b = \frac{\sqrt{2}\pi}{J}$. The state appears to be stationary when looking stroboscopically after complete driving cycles.

2. Leapfrogging states

A state starting in site $(m, \pm 1)$ moves to site $(m \mp 1, \mp 1)$ during the first phase and then to site $(m \mp 2, \pm 1)$ during the second phase. The states move two unit cells in each cycle.

3. Reflection at the corner

The two preceding paragraphs described the evolution of states in an infinite system or the bulk of finite chains. Now, we will investigate the effects of borders. The bottom left corner comprises the complete unit cell $m = 1$. The upper right corner is a partial unit cell $m = N$, containing only the site $(N, 0)$ with sites $(N, \pm 1)$ absent.

For the Hamiltonian at the edge, one needs to consider only two sites during each driving phase (instead of three for the bulk),

$$H = \begin{pmatrix} V & J \\ J & V \end{pmatrix}. \tag{21}$$

The eigenenergies are

$$E_{1,2} = V \pm J \tag{22}$$

and the eigenstates are

$$\varphi_{1,2} = \begin{pmatrix} 1 \\ \pm 1 \end{pmatrix}. \tag{23}$$

We can now write any time-dependent state during that driving phase as

$$\psi(t) = \sum_{h=1}^{2} c_h \exp(-\mathrm{i}E_h t)\varphi_h. \tag{24}$$

Without loss of generality, we initialize the state as $\psi(0) = (1, 0)^{\mathsf{T}}$. The coefficients become $c_1 = c_2 = 1/2$, resulting in

$$\psi(t) = \exp(-\mathrm{i}Vt)\begin{pmatrix} \cos(Jt) \\ -\mathrm{i}\sin(Jt) \end{pmatrix} \tag{25}$$

and the probability

$$p(t) = |\psi(t)|^2 = \begin{pmatrix} \cos^2(Jt) \\ \sin^2(Jt) \end{pmatrix}. \tag{26}$$

Compared to the three-site Hamiltonian in Sec. III, the oscillation frequency of the two-site Hamiltonian is decreased from $\sqrt{2}J$ to J. Therefore, at the end of the phase $t_a = \frac{\pi}{\sqrt{2}J}$, the state is incompletely transferred from one site to the next,

$$p(t_a) = \begin{pmatrix} \cos^2\left(\pi/\sqrt{2}\right) \\ \sin^2\left(\pi/\sqrt{2}\right) \end{pmatrix} \approx \begin{pmatrix} 0.3669 \\ 0.6331 \end{pmatrix}. \tag{27}$$

The corner influences the stationary state starting at site $(1, 0)$. It leaks into $(1, 1)$ in the first phase, from where it continues to $(2, -1)$ in the second phase. It also leaks into $(1, -1)$ in the second phase. The stationary state sends out leapfrogging states until it vanishes. Here, we described the edge at $m = 1$, but the behavior at the other edge is equivalent.

The leapfrogging states split up when they run into an edge, similar to the stationary states.

4. Interpretation as a spin-1 system

Labeling sites in the unit cell as -1, 0, and 1 already suggests an analogy to a spin-1 system. The leapfrogging states undergo a spin-flip operation from ± 1 to ∓ 1 in each phase, accompanied by a spatial movement. The spin 0 states are unaffected by the spin-flip and remain in the same location. Experimentally, this could be achieved by moving particles with a time- and space-dependent magnetic field.

Although there is a similarity to the quantum spin Hall effect in that the transport direction depends on the spin, there

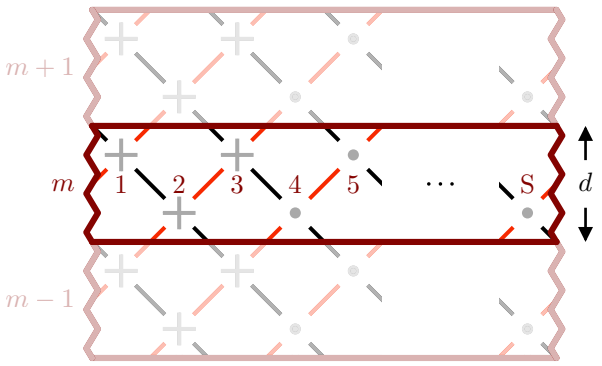

FIG. 8. Unit cell of the 45°-rotated system. The sites within it are numbered by $\alpha = 1, 2, 3, \ldots, S$ with even S. The crosses mark the diagonal sites and the dots mark the nondiagonal sites. The unit cell is infinitely repeated in the vertical direction and numbered by the index m. The height of the unit cell, d, is marked. Periodic boundaries are employed horizontally, connecting sites S and 1 within the same unit cell.

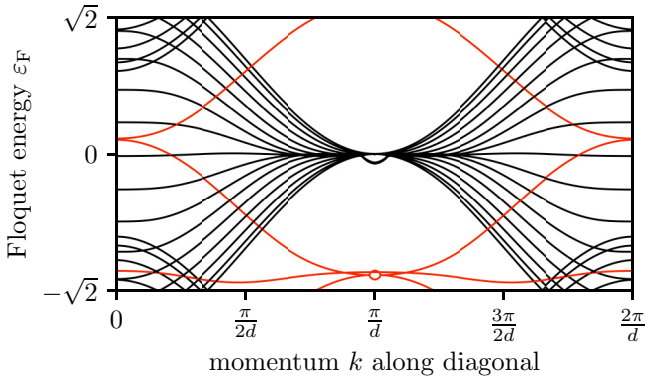

FIG. 9. Band structure of a 20-site wide strip with $V = 10$. The red bands reside on the three sites with the modified potential and the black bands on other sites.

are essential differences. While the spin remains unchanged in the spin Hall effect, it flips during transport in our model.

B. Band structure

Calculating a band structure in the one-dimensional system described in Sec. II is impossible due to the particles' interaction. After the mapping to 2D, we can calculate a band structure. To do so, we use a unit cell (shown in Fig. 8), which contains nondiagonal sites in addition to the three diagonal sites. The sites are numbered $\alpha = 1, 2, 3, \ldots, S$ with even S. The unit cell is repeated infinitely in one direction and numbered by an index m. We employ periodic boundary conditions in the other, finite direction, connecting the left and right edges of the unit cell. While this periodicity does not exist in the complete 2D system, the alternative would create diagonal edges, which do not exist in the 2D square system since there are only horizontal and vertical edges. The edge states at these diagonal edges would obfuscate the bands we are interested in.

We can write the Hamiltonians for the two phases of the driving cycle in real space as

$$\hat{H}_i = \sum_m \left(J \sum_{\alpha \text{ odd}} (\hat{h}_i(m,\alpha) + \text{H.c.}) + V \sum_{\alpha=1}^{3} |m,\alpha\rangle\langle m,\alpha| \right), \tag{28}$$

with

$$\begin{aligned} \hat{h}_a(m,\alpha) &= |m,\alpha\rangle\langle m,(\alpha-1) \mod S| \\ &\quad + |m,\alpha\rangle\langle m+1,(\alpha+1) \mod S|, \\ \hat{h}_b(m,\alpha) &= |m,\alpha\rangle\langle m,(\alpha+1) \mod S| \\ &\quad + |m,\alpha\rangle\langle m+1,(\alpha-1) \mod S|. \end{aligned} \tag{29}$$

We transform the Hamiltonians to k space by making the Bloch ansatz [18]

$$|m,\alpha\rangle = \frac{d}{2\pi} \int_{\text{BZ}} \mathrm{d}k \, \exp(-\mathrm{i}kmd) \, |k,\alpha\rangle, \tag{30}$$

where d is the lattice constant in the vertical direction in Fig. 8. We obtain

$$\hat{H}_i = \frac{d}{2\pi} \int_{\text{BZ}} \mathrm{d}k \, |k\rangle\langle k| \left(J \sum_{\alpha \text{ odd}} (\hat{h}_i(k,\alpha) + \text{H.c.}) + V \sum_{\alpha=1}^{3} |\alpha\rangle\langle\alpha| \right), \tag{31}$$

with

$$\begin{aligned} \hat{h}_a(k) &= |\alpha\rangle\langle\alpha-1| + \exp(\mathrm{i}ka)|\alpha\rangle\langle\alpha+1|, \\ \hat{h}_b(k) &= |\alpha\rangle\langle\alpha+1| + \exp(\mathrm{i}ka)|\alpha\rangle\langle\alpha-1|. \end{aligned} \tag{32}$$

The time evolution operator is

$$\hat{U}(T) = \exp\left(\frac{T}{2\mathrm{i}}\hat{H}_b\right) \exp\left(\frac{T}{2\mathrm{i}}\hat{H}_a\right). \tag{33}$$

Solving the equation

$$\hat{U}(T)\psi_F = \lambda_F \psi_F \tag{34}$$

gives the Floquet [19] eigenstates ψ_F and the Floquet energies ε_F are calculated from the eigenvalues $\lambda_F = \exp(-\mathrm{i}\varepsilon_F T)$.

The resulting band structure in Fig. 9 confirms our previous observations on the behavior of the doublons. They are located on the three sites $\alpha = 1, 2, 3$, and Floquet eigenstates where this is the case are drawn red in Fig. 9. One of these doublon bands is quite flat, corresponding to the stationary doublons. The two sloped bands correspond to doublons moving in opposite directions along the diagonal. The other bands are shown in black and form a continuum for $N \to \infty$. These bands are the diffusing states.

Depending on the potential V, some diffusing bands have nonzero energy at the center of the Brillouin zone, $\varepsilon_F(k = \frac{\pi}{d}) \neq 0$. These are edge states localized at the boundary between $\alpha = 3$ and 4 and between $\alpha = S$ and 1.

Figure 10 shows the Floquet energies $\varepsilon_F(k = \frac{\pi}{d})$ as a function of potential V. The bulk states are at constant $\varepsilon_F(k = \frac{\pi}{d}) = 0$. The energies of the doublons increase linearly with V, as indicated by the orange shadow around $\varepsilon_F = V$. The energies of the edge states show an interesting behavior: they have a tilted pole at $V \approx 3$, where they approach

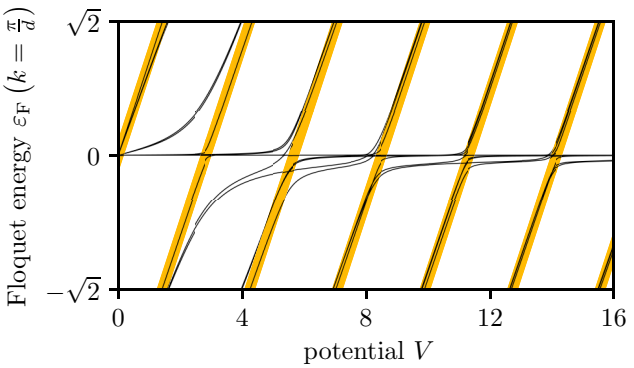

FIG. 10. Floquet energies ε_F at $k = \frac{\pi}{d}$ as a function of potential V for a 20-site wide strip. The energies of the doublons are marked by an orange shadow at $\varepsilon_F = V$.

the doublon energies. At higher potentials, they approach the energy of the bulk states, $\lim_{V\to\infty} \varepsilon_F(k = \frac{\pi}{d}) = 0$. There are crossings between the doublon and edge state energies. We have checked that they are avoided crossings by following the Floquet eigenstates.

V. POSSIBLE EXPERIMENTS AND APPLICATIONS

Ultracold atoms in optical lattices [20,21] suggest themselves for an experimental realization of our model system. The correspondence between our Floquet model and its realization in an optical lattice is readily apparent. The moving particles are the cold atoms. The sites of the lattice in the model are the sites of the optical lattice, which traps the ultracold atoms. The interaction between the two atoms can be finely tuned using Feshbach resonances [22]. Bound atom pairs have been demonstrated in periodically driven lattices [23] and for repulsive interaction in static optical lattices [24]. Modulation of the lasers achieves a change of the lattice, which enables the temporal modulation of the hoppings. Many Floquet systems have been implemented in optical lattices [25]. The use of Floquet engineering to modify the band structures of temporally periodic systems of ultracold atoms has been studied in both theory [26] and experiment [27]. Thouless pumping is one of the transport regimes that have been implemented in optical lattices [28,29]. A recent report [13] shows the implementation of interaction-induced Thouless pumping of fermionic ^{40}K atoms in an optical lattice. In their experiments, the interacting particles may be located on the same lattice sites (in contrast to our model). The periodic driving also differs. Nevertheless, the experiments suggest that our model could be implemented in optical lattices.

Another implementation would be possible in photonic waveguides [30–34]. The photonic waveguides are written into a glass block; they constitute the lattice sites. The propagation dimension of the light pulses (which are the particles) corresponds to the temporal dimension. Hopping amplitudes can be modified by changing the distance between waveguides or turned on and off by writing "blockers" between them. Directly implementing the two one-dimensional chains would be challenging to realize experimentally because of the necessary interaction between particles (light pulses) on neighboring sites. The two-dimensional square lattice (after mapping to two dimensions as described in Sec. IV) is more suitable for experimental realization. The different potentials of its lattice sites are implemented as different refractive indices of the respective waveguides. Solitons and edge states have been achieved experimentally [35–39] and also Thouless pumping [40].

VI. CONCLUSION AND SIGNIFICANCE

We investigated two particles on two linear chains in a periodic driving scheme and showed how their interaction influences their temporal evolution. Without interaction, both particles diffuse. With sufficiently strong interaction, they can form a stationary bound state that remains localized without diffusing. They can also form nonstationary, nondiffusing states, which propagate in a leapfrogging manner. These states are energetically separated from all others, as seen in the Floquet band structure. The relative position of the two particles in the starting configuration determines their behavior.

A possible extension of the system would be going from linear chains to two-dimensional grids on which the particles move. The added dimension would enable vertical and diagonal movement of the particles in addition to the horizontal one on the chains.

Our relatively simple model system harbors spatially localized states, which are only stable due to interaction. We think of it as a building block, a part of a toolbox for synthetic quantum systems. We envision its potential use for transporting two particles together for some distance and then splitting them up again at the target location. This could be useful for information transfer in quantum computing. Entangling particles (e.g., their spins) before their transport would also be possible.

Observing the evolution of the two particles and the lifetime of their bound state could allow us to measure the strength of the interaction between them. Since the direction of transport depends on the exact initial locations of the two particles, the system could be used as a switch in quantum computing, relaying signals to the left or to the right depending on the input.

ACKNOWLEDGMENTS

This research and publication were supported by the Studienstiftung des deutschen Volkes (German Academic Scholarship Foundation) and the Deutsche Forschungsgemeinschaft (DFG, German Research Foundation), SFB 1477 "Light-Matter Interactions at Interfaces," Project No. 441234705.

[1] E. H. Hall, On a new action of the magnet on electric currents, Am. J. Math. **2**, 287 (1879).

[2] M. I. Dyakonov and V. I. Perel, Current-induced spin orientation of electrons in semiconductors, Phys. Lett. A **35**, 459 (1971).

[3] D. R. Hofstadter, Energy levels and wave functions of Bloch electrons in rational and irrational magnetic fields, Phys. Rev. B **14**, 2239 (1976).

[4] K. von Klitzing, T. Chakraborty, P. Kim, V. Madhavan, X. Dai, J. McIver, Y. Tokura, L. Savary, D. Smirnova, A. M. Rey, C. Felser, J. Gooth, and X. Qi, 40 years of the quantum Hall effect, Nat. Rev. Phys. **2**, 397 (2020).

[5] P. Reimann, Brownian motors: noisy transport far from equilibrium, Phys. Rep. **361**, 57 (2002).

[6] P. Hänggi and F. Marchesoni, Artificial Brownian motors: Controlling transport on the nanoscale, Rev. Mod. Phys. **81**, 387 (2009).

[7] S. Yukawa, M. Kikuchi, G. Tatara, and H. Matsukawa, Quantum Ratchets, J. Phys. Soc. Jpn. **66**, 2953 (1997).

[8] P. Reimann, M. Grifoni, and P. Hänggi, Quantum ratchets, Phys. Rev. Lett. **79**, 10 (1997).

[9] N. Dupont, L. Gabardos, F. Arrouas, N. Ombredane, J. Billy, B. Peaudecerf, and D. Guéry-Odelin, Hamiltonian ratchet for matter-wave transport, Phys. Rev. Lett. **131**, 133401 (2023).

[10] D. J. Thouless, Quantization of particle transport, Phys. Rev. B **27**, 6083 (1983).

[11] R. Citro and M. Aidelsburger, Thouless pumping and topology, Nat. Rev. Phys. **5**, 87 (2023).

[12] A.-S. Walter, Z. Zhu, M. Gächter, J. Minguzzi, S. Roschinski, K. Sandholzer, K. Viebahn, and T. Esslinger, Quantization and its breakdown in a Hubbard-Thouless pump, Nat. Phys. **19**, 1471 (2023).

[13] K. Viebahn, A.-S. Walter, E. Bertok, Z. Zhu, M. Gächter, A. A. Aligia, F. Heidrich-Meisner, and T. Esslinger (unpublished).

[14] L. Lin, Y. Ke, and C. Lee, Interaction-induced topological bound states and Thouless pumping in a one-dimensional optical lattice, Phys. Rev. A **101**, 023620 (2020).

[15] B. N. Narozhny and A. Levchenko, Coulomb drag, Rev. Mod. Phys. **88**, 025003 (2016).

[16] A. Slavík and P. Stehlík, Explicit solutions to dynamic diffusion-type equations and their time integrals, Appl. Math. Comput. **234**, 486 (2014).

[17] See Supplemental Material at http://link.aps.org/supplemental/10.1103/PhysRevResearch.6.023032 for a video of the evolution of the probabilities for increasing interaction V going from the spreading at $V = 0$ (Fig. 5) to the periodic returns at $V \gg J$ (Fig. 2).

[18] F. Bloch, Über die Quantenmechanik der Elektronen in Kristallgittern, Z. Phys. **52**, 555 (1929).

[19] G. Floquet, Sur les équations différentielles linéaires à coefficients périodiques, Ann. Sci. École Norm. Sup. **12**, 47 (1883).

[20] R. Grimm, M. Weidemüller, and Y. B. Ovchinnikov, in *Optical Dipole Traps for Neutral Atoms*, edited by B. Bederson and H. Walther, Advances In Atomic, Molecular, and Optical Physics Vol. 42 (Academic Press, New York, 2000), pp. 95–170.

[21] I. Bloch, Ultracold quantum gases in optical lattices, Nat. Phys. **1**, 23 (2005).

[22] C. Chin, R. Grimm, P. Julienne, and E. Tiesinga, Feshbach resonances in ultracold gases, Rev. Mod. Phys. **82**, 1225 (2010).

[23] H.-H. Zhong, Z. Zhou, B. Zhu, Y.-G. Ke, and C.-H. Lee, Floquet bound states in a driven two-particle bose-hubbard model with an impurity, Chin. Phys. Lett. **34**, 070304 (2017).

[24] K. Winkler, G. Thalhammer, F. Lang, R. Grimm, J. Hecker Denschlag, A. J. Daley, A. Kantian, H. P. Büchler, and P. Zoller, Repulsively bound atom pairs in an optical lattice, Nature (London) **441**, 853 (2006).

[25] C. Weitenberg and J. Simonet, Tailoring quantum gases by Floquet engineering, Nat. Phys. **17**, 1342 (2021).

[26] M. Holthaus, Floquet engineering with quasienergy bands of periodically driven optical lattices, J. Phys. B: At. Mol., Opt. Phys. **49**, 013001 (2016).

[27] C. J. Fujiwara, K. Singh, Z. A. Geiger, R. Senaratne, S. V. Rajagopal, M. Lipatov, and D. M. Weld, Transport in floquet-bloch bands, Phys. Rev. Lett. **122**, 010402 (2019).

[28] S. Nakajima, T. Tomita, S. Taie, T. Ichinose, H. Ozawa, L. Wang, M. Troyer, and Y. Takahashi, Topological Thouless pumping of ultracold fermions, Nat. Phys. **12**, 296 (2016).

[29] M. Lohse, C. Schweizer, O. Zilberberg, M. Aidelsburger, and I. Bloch, A Thouless quantum pump with ultracold bosonic atoms in an optical superlattice, Nat. Phys. **12**, 350 (2016).

[30] K. Itoh, W. Watanabe, S. Nolte, and C. B. Schaffer, Ultrafast processes for bulk modification of transparent materials, MRS Bull. **31**, 620 (2006).

[31] A. Szameit and S. Nolte, Discrete optics in femtosecond-laser-written photonic structures, J. Phys. B: At. Mol. Opt. Phys. **43**, 163001 (2010).

[32] M. C. Rechtsman, J. M. Zeuner, Y. Plotnik, Y. Lumer, D. Podolsky, F. Dreisow, S. Nolte, M. Segev, and A. Szameit, Photonic Floquet topological insulators, Nature (London) **496**, 196 (2013).

[33] T. Ozawa, H. M. Price, A. Amo, N. Goldman, M. Hafezi, L. Lu, M. C. Rechtsman, D. Schuster, J. Simon, O. Zilberberg, and I. Carusotto, Topological photonics, Rev. Mod. Phys. **91**, 015006 (2019).

[34] H. Price, Y. Chong, A. Khanikaev, H. Schomerus, L. J. Maczewsky, M. Kremer, M. Heinrich, A. Szameit, O. Zilberberg, Y. Yang, B. Zhang, A. Alù, R. Thomale, I. Carusotto, P. St-Jean, A. Amo, A. Dutt, L. Yuan, S. Fan, X. Yin, C. Peng, T. Ozawa, and A. Blanco-Redondo, Roadmap on topological photonics, J. Phys. Photon. **4**, 032501 (2022).

[35] Y. Lumer, Y. Plotnik, M. C. Rechtsman, and M. Segev, Self-localized states in photonic topological insulators, Phys. Rev. Lett. **111**, 243905 (2013).

[36] M. J. Ablowitz, C. W. Curtis, and Y.-P. Ma, Linear and nonlinear traveling edge waves in optical honeycomb lattices, Phys. Rev. A **90**, 023813 (2014).

[37] D. Leykam and Y. D. Chong, Edge solitons in nonlinear-photonic topological insulators, Phys. Rev. Lett. **117**, 143901 (2016).

[38] S. Mukherjee and M. C. Rechtsman, Observation of Floquet solitons in a topological bandgap, Science **368**, 856 (2020).

[39] S. Mukherjee and M. C. Rechtsman, Observation of unidirectional solitonlike edge states in nonlinear floquet topological insulators, Phys. Rev. X **11**, 041057 (2021).

[40] M. Jürgensen, S. Mukherjee, C. Jörg, and M. C. Rechtsman, Quantized fractional Thouless pumping of solitons, Nat. Phys. **19**, 420 (2023).